Extending yield-stress fluid paradigms

Arif Z. Nelson, Rafael E. Bras, Jingping Liu, and Randy H. Ewoldt

Citation: Journal of Rheology **62**, 357 (2018); doi: 10.1122/1.5003841
View online: https://doi.org/10.1122/1.5003841
View Table of Contents: http://sor.scitation.org/toc/jor/62/1
Published by the The Society of Rheology

Extending yield-stress fluid paradigms

Arif Z. Nelson

Department of Mechanical Science and Engineering, University of Illinois at Urbana-Champaign, Urbana, Illinois 61801

Rafael E. Bras and Jingping Liu

Wm. Wrigley Jr. Company, 1132 W. Blackhawk Street, Chicago, Illinois 60642

Randy H. Ewoldt[a)]

Department of Mechanical Science and Engineering, University of Illinois at Urbana-Champaign, Urbana, Illinois 61801

(Received 7 September 2017; final revision received 13 November 2017; published 3 January 2018)

Abstract

We report experimental measurements of high extensibility of several yield-stress fluids, demonstrating a behavior completely outside the standard paradigm of model materials and constitutive equations for yield-stress fluids. We identify "highly" extensible materials using uniaxial tension tests, as materials with values of strain-to-break larger than predictions from the tensorial Herschel-Bulkley model, and larger strain-to-break than some of the most studied model materials including aqueous microgel particle suspensions (Carbopol), and aqueous clay suspensions (Laponite and Bentonite). Materials in commercial use, including a printing resin, chewing gums, and food products, have a yield stress but do not rupture until reaching extremely large extensional deformations. The purpose of this work is to introduce a method for characterizing the extensibility of yield-stress fluids, demonstrate the range of extensibility seen in real yield-stress fluids (commercial products, biomaterials), and introduce one possible model material for highly extensible yield-stress fluids: Silicone oil droplets emulsified at moderate volume fraction into an aqueous solution of polyvinyl alcohol cross-linked by sodium tetraborate. © *2018 The Society of Rheology*. https://doi.org/10.1122/1.5003841

I. INTRODUCTION

The rheologically complex phenomenon of the yield-stress fluid, which transitions from solidlike to liquidlike behavior upon a critical applied stress [1], is an enabler of applications both mundane and marvelous. The phenomenon applies to products that many use every day such as peanut butter and toothpaste, but it is also extremely important for a multitude of industrial applications such as the manufacturing of foodstuffs and 3D printing [2–4]. It is no surprise therefore, yield-stress fluids have been the subject of substantial rheological characterization and study [1,2,5–7].

However, as shown in Fig. 1, there is an obvious discrepancy in the extensional behavior between well-studied laboratory yield-stress fluids [Fig. 1(A)] [8] and common industrial and consumer yield-stress fluid materials [Figs. 1(B) and 1(C)]. Figures 1(A) and 1(B) depict the materials immediately after rupture occurs. When compared to model materials, the application-relevant yield-stress fluids are often able to survive enormous extensional strains. Due to this discrepancy, we suggest a silicone oil-in-water emulsion with a transiently crosslinked network of poly(vinyl alcohol) as a model for studying the behavior of highly extensible yield-stress fluids [Fig. 1(D)].

In bubble gum [Fig. 1(C)], it is important that the material be able to reach large extensional strains because this contributes to consumer perception as well as the ability to blow bubbles [9]. To the authors' knowledge, the importance of high-extensibility has not been directly established for applications involving printing of yield-stress fluids such as the resin shown in Fig. 1(B). Though not the focus of this work, it has been conjectured that a printed filament of highly extensible material will not rupture as easily during extrusion, contributing to a smoother and more desirable surface finish [10].

While previous studies of yield-stress fluids have been extensive, none have conceived of the materials as being highly extensible. There are certainly many yield-stress fluids that cannot survive large extensional strains. However, the works investigating yield-stress fluids in extension do not recognize materials that *are* able to reach large strains, instead typically focusing on more pastelike yield-stress fluids [11]. Yield-stress fluids in extension have been of interest for understanding the pinch off dynamics in a separating plate [12–14] and drop formation configuration [15], and to measure critical flow and separation stresses in extension [16–18]. The lack of studies on highly extensible yield-stress fluids is an imbalance in the current paradigm which we

[a)]Author to whom correspondence should be addressed; electronic mail: ewoldt@illinois.edu

hope to rectify here by (i) demonstrating the extent to which common model materials differ from real materials in terms of extensibility, and (ii) introducing a simply formulated material that is both highly extensible and has a yield stress [Fig. 1(D)].

II. BACKGROUND

A. Extensional rheology and properties

The importance of characterizing the extensional properties of various materials has been widely recognized for polymer processing with polymer solutions and melts [20–24], biological fluids such as saliva [25], magnetic industrial fluids used in vibration dampers [26], surface coatings [14], food materials [12], and consumer confectionary products such as chewing gum [9,27]. For the characterization of the uniaxial extensional properties of these materials, the most common methods are the imposition of either a constant extensional strain rate or a step extensional displacement (filament stretching or capillary breakup) [20,28]. Here, we characterize materials by imposing a constant extensional strain-rate to measure the strain at which rupture occurs (strain-to-break). The two methods by which we impose extensional strain rates are by (i) exponentially increasing the separation velocity of two parallel plates (referred to here as "filament-stretching") and (ii) using a counter-rotating-drum fixture at a fixed velocity. For the filament-stretching experiments for initial radius, R_0, and initial plate separation, H_0, the aspect ratio,

$$\Lambda_0 = H_0/R_0, \tag{1}$$

should be approximately unity for homogeneous uniaxial extensional flow [23]. The counter-rotating-drum method was used when the filament-stretching experimental setup could not access the strain-to-break of a material (due to finite travel length). The true strain (also known as Hencky strain),

$$d\varepsilon_{true} = \frac{dL}{L} \tag{2}$$

and engineering strain,

$$\varepsilon_{eng} = \frac{L_{final} - L_{initial}}{L_{initial}} \tag{3}$$

are related by [29],

$$\varepsilon_{true} = \ln(\varepsilon_{eng} + 1). \tag{4}$$

For the stability of a material in extension, the Considère criterion has been used in both solid mechanics [30] and for polymeric materials [24,31] to quantitatively predict the critical strain beyond which homogeneous extension no longer occurs. The necking behavior of some materials has been found to be strain-rate dependent [22,32], but in the limit of "fast" extension (i.e., where no molecular relaxation occurs), the critical strain of the Considère criterion has been used to predict the failure strain (strain-to-break) for constitutive equations that describe the behavior of polymer melts [33]. By this same method, it can be shown (see the Appendix) that the tensorial Herschel-Bulkley model (see Sec. II B) predicts that yield-stress fluids never undergo stable uniaxial extension (i.e., have a critical strain value of zero). Thus, this simple model fails to capture the failure strains shown in Figs. 1(B) and 1(C).

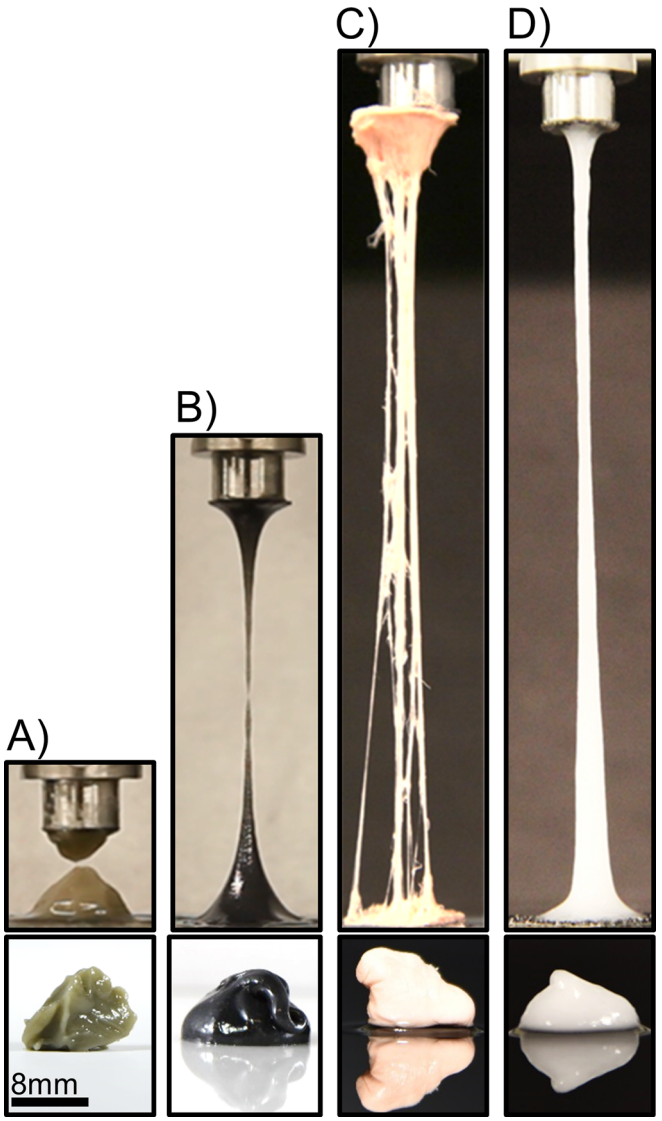

FIG. 1. The extensional behavior of yield-stress fluids. (A) Bentonite clay suspension, a commonly studied material that fails to match the extensibility of other yield-stress fluids; (B) a resin used in printing by the company HexArmor; (C) the bubble gum, Hubba Bubba Bubble Tape; and (D) a model material introduced here. The scale bar shown applies to all images. See Supplementary Material for the videos of these filament stretching tests (adapted from [19]).

Of course, it must be noted that the strain-to-break is an *extrinsic* material property that may vary for different initial geometries. This is not to diminish the importance of this parameter, as it is extremely useful in solid mechanics for informing material selection choices by comparing the ductility of materials through their "percent elongation" [34]. However, just as in the characterization of solid materials, care must be taken when comparing materials to standardize the initial sample geometry and extension rate, which we do here as much as possible.

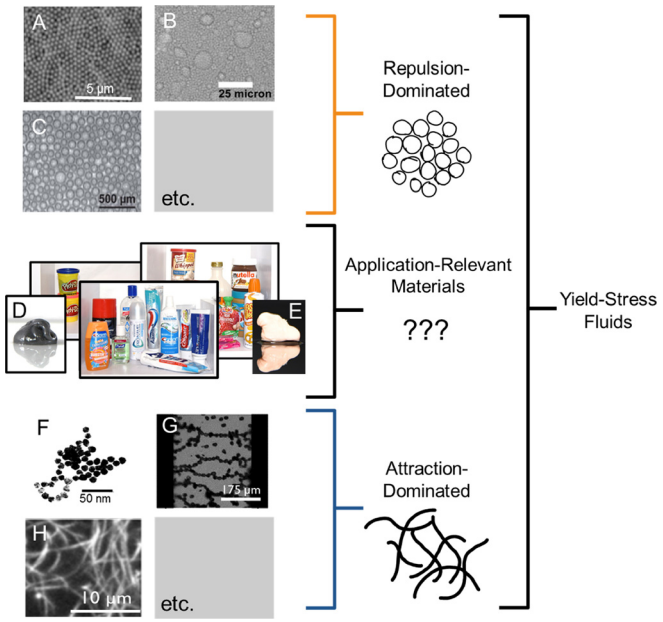

FIG. 2. The many microstructures of yield-stress fluids, organized into "repulsion-dominated" and "attraction-dominated" (although combinations also exist), adapted from [19]. For most application-relevant materials, the microstructural mechanism governing the yield stress is unknown. Materials pictured include toothpaste, shaving cream, playdoh, spray cheese, and apple sauce, all of which are yield-stress fluids. Images shown are (A) particulate suspension [38], (B) emulsion [39], (C) foam [40], (D) HexArmor resin, (E) Hubba Bubba Bubble Tape, (F) particulate gel [41], (G) electro/magneto-rheological fluid [42], and (H) fiber gel [43].

B. Yield-stress fluids

Though it has been debated whether a "true" yield stress fluid exists, the concept has been accepted as a practical reality for most applications, with definitions hinging on the critical value of stress that must be reached to fluidize the material [1,6,35]. Controversy over the true existence of yield-stress fluids arises from experimental observations of extremely slow flow even below any critical stress value [2], but on the timescales of many applications this deformation is not significant. Additionally, there are numerous ways in which a yield-stress may be characterized which are the focus of several reviews [3,36,37]. Regardless of the characterization method, it is generally true that there is no sharp transition in flow behavior, and thus "the yield stress" is actually representative of a (typically narrow) region of stresses where the material behavior dramatically transitions.

TABLE I. Archetypal yield-stress fluid formulations organized by material and weight-percentage of additives. In all cases, remaining wt. % is of water. Specific synthesis methods are the same as originally published in the Supplementary Information of Nelson & Ewoldt [19].

	wt. % Solid content	
Carbopol	0.1, 0.15, 0.2, 0.25, 0.5	
Bentonite	7, 8, 9, 10, 11, 12	
Laponite	3, 4, 5	
Xanthan Gum	2, 4, 5	
	wt. % Oil	wt. % SDS
Silicone oil-in-water emulsion	65	11.7
	70	10
	75	8.3
	80	6.7
Mineral oil-in-water emulsion	65	11.7
	75	8.3

TABLE II. Proposed model material formulations. In all cases, poly(vinyl alcohol) and borax content was supplied from 4 wt. % stock solutions in water. For specific synthesis procedure refer to Sec. III.

	wt. % Oil	wt. % PVA	wt. % Borax	vol. % Oil
PVA-borax emulsion	50	1	1	51
	55	0.9	0.9	56
	60	0.8	0.8	61

For this paper, yield-stress characterization is performed in one of two ways depending on the sample: Either velocity-controlled steady flow tests or step-stress creep compliance tests. Data from the velocity-controlled steady flow experiments were fit to the three-parameter Herschel-Bulkley model

$$\sigma = \sigma_Y + K\dot{\gamma}^n, \tag{5}$$

which we prefer to rewrite [19] as

$$\sigma = \sigma_Y\left[1 + \left(\frac{\dot{\gamma}}{\dot{\gamma}_{critical}}\right)^n\right], \tag{6}$$

to obtain the yield-stress, σ_Y, and critical shear rate, $\dot{\gamma}_{critical}$ (shear rate at which the stress is double the yield-stress), whose dimensions are independent of n.

There are numerous chemistries and microstructures capable of producing a yield-stress fluid; however, materials can typically be organized into two categories based on the structural mechanism by which the yield stress comes about [19]. As shown in Fig. 2, for repulsion-dominated materials the yield stress comes about by microstructural jamming, yielding once the structure is able to rearrange and slide past itself. For attraction-dominated materials, the yield stress comes about primarily by the microstructure resisting being pulled apart, yielding once these reformable attractions have been broken. However, combinations of both mechanisms are of course possible and it is there that most consumer products with complex formulations are likely to exist, although frequently the microstructure is simply unknown.

III. MATERIALS AND METHODS

Materials include well-studied *archetypal* yield-stress fluids (materials one may regard as "classic" yield-stress fluids within rheological literature), commercial products, and a new model material that we propose for yield-stress fluids with extensibility (refer to Tables I and II for the specific material formulations presented in this paper). The preparation of the archetypal yield-stress fluids is the same as detailed in the supplementary information of Nelson & Ewoldt 2017 [19].

For our proposed model material, hereafter referred to as a polyvinyl alcohol (PVA)-borax emulsion, 1000 cSt silicone oil with a density of 0.97 g/ml obtained from Sigma Aldrich

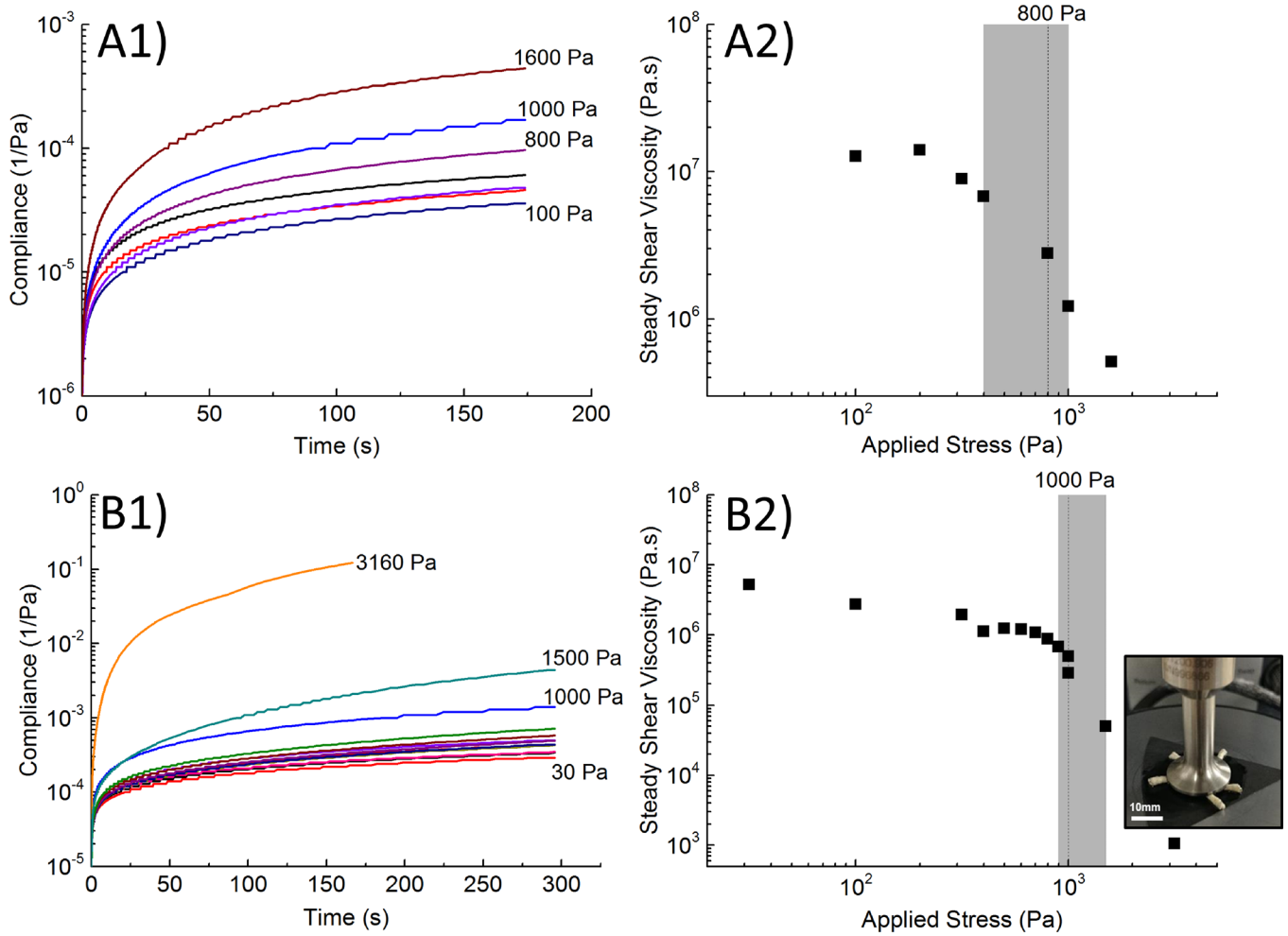

FIG. 3. Shear creep compliance curves for difficult-to-test materials, (A) Laffy Taffy, and (B) Hubba Bubba Bubble Tape. Velocity-controlled flow tests were not feasible for these materials due to edge failure behavior [inset image in (B2)]. Constant applied stress tests were used to obtain the compliance over time, with the applied stresses increasing monotonically between the labeled compliance curves [(A1) and (B1)]. From the compliance, the resulting steady shear viscosity curves [(A2) and (B2)] show gradual yielding. The gray shaded regions identify the stresses over which viscosity has begun to decrease substantially, the yield stress for each material is taken as the stress for the data point within the shaded regions. Error bars are smaller than data points.

was blended using an overhead stirrer at 600 rpm for 5 min with a 4 wt. % solution of poly(vinyl alcohol) (molecular weight 85 000–124 000, 99+% hydrolyzed) in deionized water and then added to a test tube containing a 4 wt. % solution of sodium tetraborate in deionized water and shaken vigorously and occasionally stirred for 5 min. The overall weight-percentages of the oil, PVA, and sodium tetraborate were varied as detailed in Table II. The poly(vinyl alcohol) and sodium tetraborate were both purchased from Sigma-Aldrich. Using the density of the oil and assuming the continuous phase has approximately the same density as water, lower bound estimates of the volume fraction are obtained and are given in Table II. It is possible that the adsorption of PVA at the oil-water interface results in a larger effective volume fraction [44], but this is unconfirmed and outside the scope of this work. Additionally, the chosen mixing method likely entrains air bubbles that contribute to the jammed volume fraction.

The industry-relevant products tested were Nutella Hazelnut Spread (Ferrero), Whipped Frosting (Duncan Hines), Laffy Taffy (Nestlé), Hubba Bubba Bubble Tape (Wm. Wrigley Jr. Company), resin used in the production of HexArmor personal protective equipment, and Mystic Smoke (a material used in performance magic, Loftus International). Before testing, the Hubba Bubba Bubble Tape was chewed for 20 min, at which point the weight of the material ceased to depend on chewing time. All other consumer products were tested as received. Unless noted otherwise, all rheological experiments were repeated three times.

Rheological characterization for the yield stress was performed on a TA Instruments DHR-3 or AR-G2 rotational rheometer (combined motor/transducer instruments) using a parallel-plate geometry with a diameter of 20 or 40 mm. All materials were tested within one week of formulation except the Bentonite and Laponite suspensions. Bentonite and Laponite formulations were allowed to stand quiescently for one week before testing to hydrate [45]. Depending on the sample, either a sandblasted plate or adhesive-backed silicon carbide sandpaper (600 or 60 grit) was used to prevent slip. Materials were tested at multiple gaps to verify the absence of slip [36,46,47]. For velocity-controlled steady flow experiments, an apparent shear rate was applied and the resulting

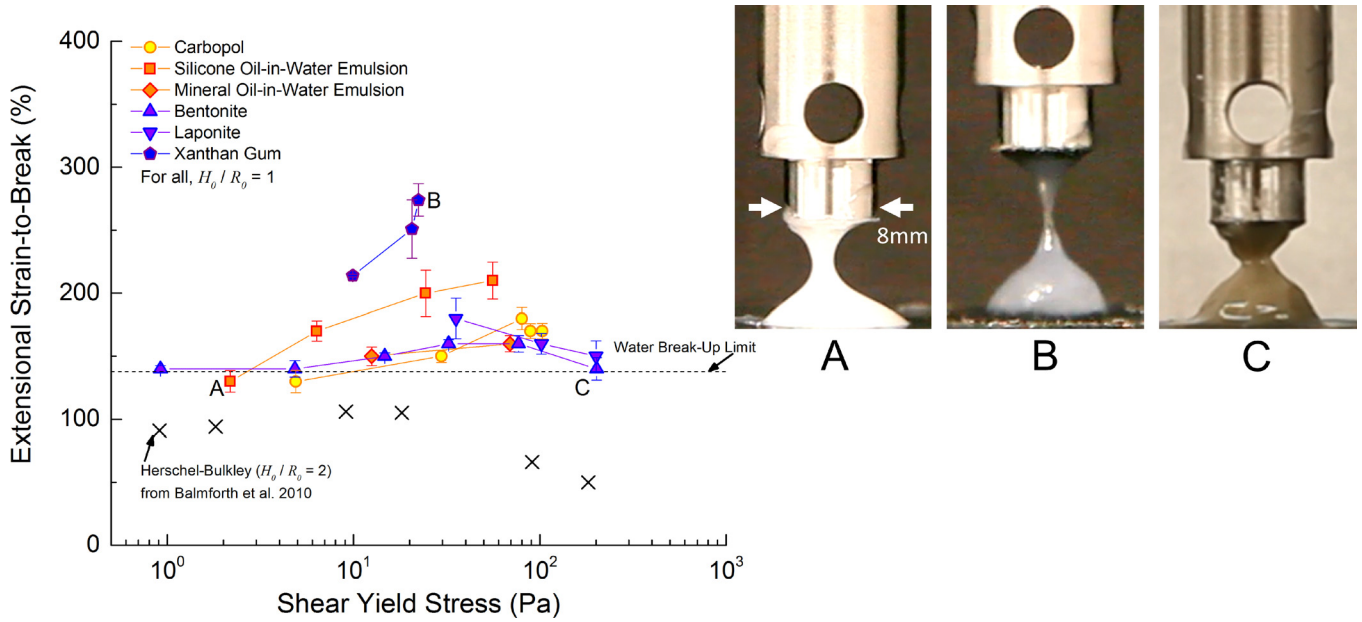

FIG. 4. Ashby-style co-plot of the shear and extensional behavior of archetypal yield-stress fluids. All filament stretching tests were performed with an initial aspect ratio, $\Lambda_0 = H_0/R_0 = 1$. Shown are three representative materials: (A) A silicone oil-in-water emulsion that is 65 wt. % oil, (B) 5 wt. % xanthan gum in water, and (C) 12 wt. % Bentonite in water. Error bars are the standard deviation from repeated experiments. The water break-up limit for a volume equivalent to those in our experiments is 135% and was determined for zero-gravity conditions [50]. The values from [13] were found using a Herschel-Bulkley model for an initial aspect ratio double that of our experiments. See Supplementary Material for the full steady shear flow and extensional engineering stress curves that these points represent.

stress measured. With decreasing gap, a slip effect manifests as a lower value of stress at each value of apparent shear rate; we see no evidence of slip unless noted, though some materials showed higher measured flow stress at a lower gap (Fig. 5), indicating a confinement effect. In all cases, reported values from model fits are taken from the largest gap height.

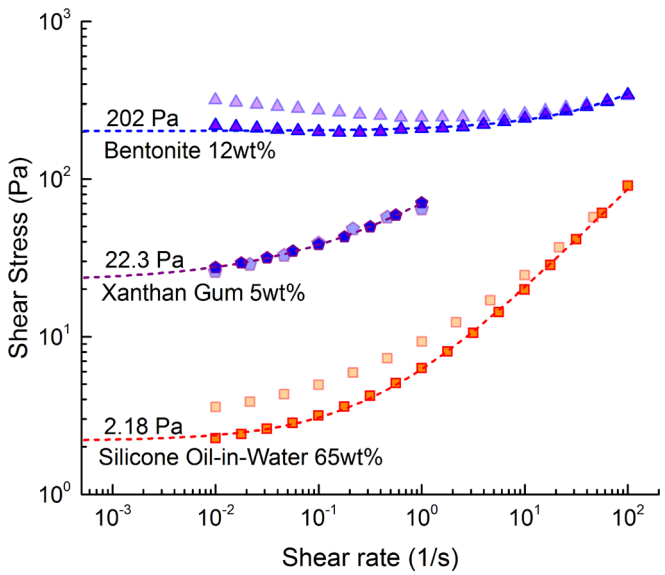

FIG. 5. Steady simple shear flow for the three representative materials shown in Fig. 4. The lightened data points are tests performed at a smaller gap, and from these tests we see no evidence of slip. Rather, a confinement effect (higher flow stress at lower gap) is observed. All yield-stress parameters are fit to the flow data at the highest tested gap. A velocity-controlled test from high-to-low shear rates was used for Bentonite and silicone oil-in-water, resulting in a dynamic yield stress. A low-to-high shear rate was used for xanthan gum, resulting in a static yield stress. For discussion of the static yield stress measurement for xanthan gum, see Supplementary Material Figure S13. The dashed lines show the fit Herschel-Bulkley model for each material.

Parallel-plate corrections were used to identify the true shear stress. Apparent stress (σ_A) values were fit to a polynomial curve and corrected to the stress at the rim using

$$\sigma_{True} = \frac{\sigma_A}{4}\left[3 + \frac{d\ln\sigma_A}{d\ln\dot{\gamma}}\right], \tag{7}$$

where $\dot{\gamma}$ is the applied shear rate [35]. Corrected stress versus shear rate data was fit to the Herschel-Bulkley model [Eq. (6)] to obtain the yield stress. Unless otherwise specified, all tests were performed starting from a high shear rate of $100\,s^{-1}$ (or the highest applicable rate without edge fracture) and successively decreasing to $0.01\,s^{-1}$, thus the yield stress is a dynamic yield stress rather than a static yield stress [8]. As the criteria for steady-state, each applied shear rate was held constant until the average stress across three successive thirty second periods varied by less than five percent. The typical time at each applied shear rate was between two and three minutes. For some materials, especially at smaller gaps, a nonmonotonic stress versus rate curve was observed, with a local minimum (Figure 5 Bentonite) [37,48]. In the case of these materials, the Herschel-Bulkley model was only fit to data at the local minimum of stress and higher shear rates (thus giving the lower bound description of a dynamic yield stress). All fitting was performed with variance weighting using OriginPro 9.0 software. See Supplementary Information for steady shear flow curves of archetypal materials, originally published in Nelson & Ewoldt [19], and of the proposed model material.

Velocity-controlled tests were problematic for materials prone to edge failure at high shear-rates, including the Laffy Taffy, Hubba Bubba Bubble Tape, and the proposed model material. For these cases, a series of step-stress creep tests

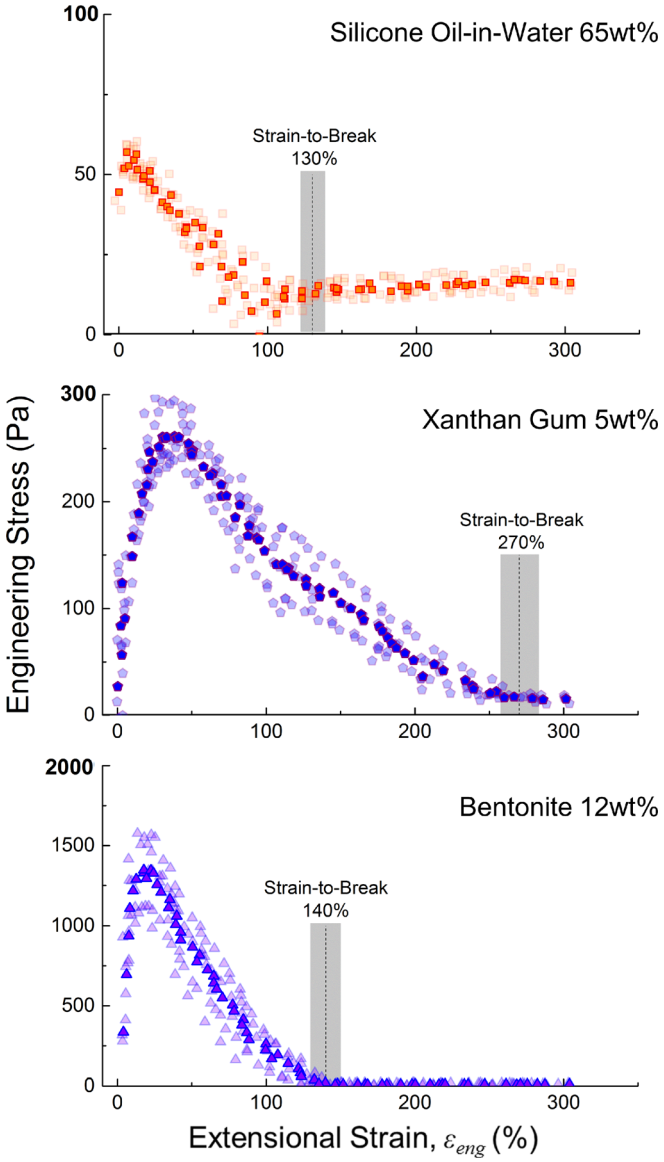

FIG. 6. Extensional engineering stress curves for the three representative materials shown in Fig. 4 tested using the ARES-G2 filament stretching experimental setup. The bold data points are the average of repeated experiments (lightened data points) The vertical dashed lines depict the average strain-to-break which was found by correlating the extensional stress curves with video images. The width of the shaded region depicts the standard deviation in the strain-to-break from repeated experiments. A constant true strain-rate of $\dot{\varepsilon} = 0.2\,\mathrm{s}^{-1}$ was used for all extensional tests.

were imposed (Fig. 3). Materials were allowed to reach a steady shear-rate, allowing for the determination of steady shear viscosity as a function of the applied stress. The yield-stress in this case was taken from within the stress range over which the viscosity declines by over a half-order of magnitude. Note that because no simple correction is available for step-stress tests with parallel disks, the yield stresses of the materials tested in creep are apparent stresses rather than true stresses.

Characterization with filament stretching for the extensional strain-to-break was performed on a TA Instruments ARES-G2 rheometer (separated rotational motor/transducer, combined axial motor/transducer). For the filament-stretching experiments, a parallel-plate geometry with a diameter of

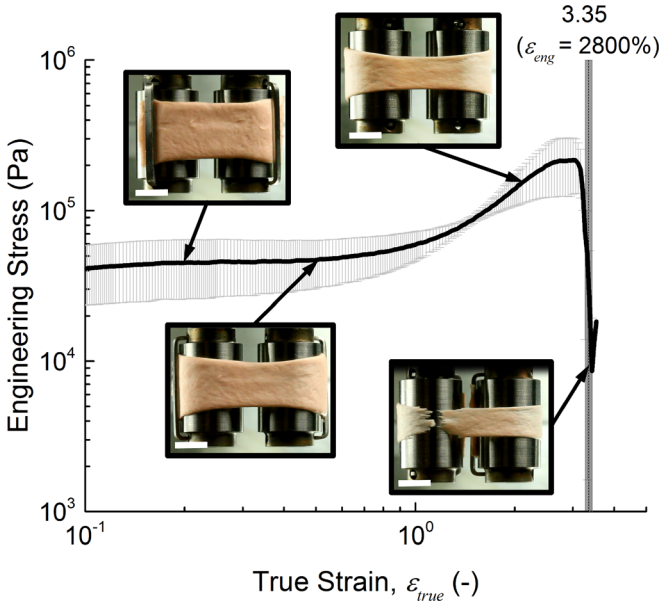

FIG. 7. Extensional engineering stress versus true strain for a commercial product, Hubba Bubba Bubble Tape. Extensional data for materials which reach the limit of extensibility for the ARES-G2 filament stretching experimental setup (shown in Fig. 1) were obtained using an SER3 counter-rotating-drum stretching experiment as shown. The white scale bar in each image is 5 mm. The dashed line indicates the strain-to-break. For comparison with other materials, the true strain was related to engineering strain with Eq. (2). The error bars are the standard deviation from repeat experiments. See Supplementary Material for video of test.

8 mm and advanced Peltier system bottom plate were used. The samples were loaded at a gap of 4 mm, resulting in an aspect ratio of $\Lambda_0 = H_0/R_0 = 1$. Samples were loaded as near to the initial height as possible to minimize compression. Samples were not presheared for extensional tests. The maximum gap on the ARES-G2 allowed for a maximum

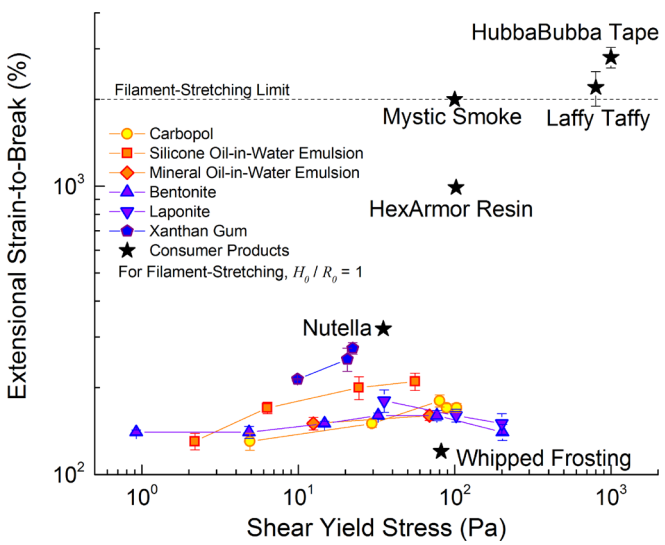

FIG. 8. Ashby-style co-plot of archetypal yield-stress fluids and consumer products. For Mystic Smoke which could not be loaded in the counter-rotating-drum setup, the filament-stretching limit is taken as the lower bound of the strain-to-break. Error bars shown are the standard deviation from repeat experiments. Note that, compared to Fig. 4, both axes are logarithmic scales. See Supplementary Material for the full steady shear flow and extensional engineering stress curves that these points represent.

engineering strain of $\varepsilon_{eng} = 2000\%$ ($\varepsilon_{true} \approx 3.04$). A constant true strain rate, $\dot{\varepsilon} = 0.2\text{s}^{-1}$, was used for all tests.

The counter-rotating-drum experiments were performed on the previously mentioned DHR-3 rotational rheometer using an SER2 or SER3 Universal Testing Platform fixture from Xpansion Instruments. For the counter-rotating-drum experiments, samples were loaded as per the recommended dimensions and procedure [21]. A constant true strain rate, $\dot{\varepsilon} = 0.2\text{s}^{-1}$, was used for all tests. Videos were taken during all extensional tests, and images were correlated with the measured load and displacement to determine the extensional strain-to-break. See Supplementary Material for all extensional stress-strain curves from both filament-stretching and counter-rotating-drum experiments [49].

For microstructural characterization of the PVA-Borax emulsion, optical microscopy with transmitted bright-field illumination was performed using a Nikon Eclipse Ti-U inverted microscope with an EM-CCD camera. Micrographs were recorded with a 20 × objective lens at various locations across multiple samples.

IV. RESULTS

A. Archetypal yield-stress fluids and consumer products

The shear and extensional behavior of the studied archetypal yield-stress fluids are shown in Fig. 4 with images of representative systems just before rupture occurs. All data points in Fig. 4 are simplified descriptions of the full data from shear flow and extensional flow (see Supplementary Material). The steady simple-shear flow characterization for the three representative systems in Fig. 4 is shown in Fig. 5, and the extensibility characterization is shown in Fig. 6. While these materials span a range in yield stresses of over two decades, the engineering strain-to-break only varies by approximately a factor of two.

As shown in Fig. 4, there is no clear correlation between the extensibility and yield-stress for the data set taken as a whole. However, correlations can be seen within distinct material systems. Carbopol and the silicone oil-in-water emulsions, both repulsion-dominated systems, show a slight increase in extensibility as their yield stresses increase, with the extensibility of Carbopol saturating at the same concentration as the measured yield stress value. The extensibility of Bentonite and of the mineral oil-in-water emulsion are essentially constant as their yield stresses are increased. Laponite is the one tested system that shows a decrease in extensibility as the yield stress is increased. Xanthan gum, a long-chain polymer system, shows the largest extensibility, as may be expected from a stretchy attractive network. However, comparing Figs. 1 and 4, the extensibility of xanthan gum shown in Fig. 4(B) is far less than the extensibility behavior seen for the application-relevant materials in Figs. 1(B) and 1(C) [though xanthan does show necking behavior somewhat similar to the printing resin in Fig. 1(B)].

The tested materials with the lowest yield-stresses rupture in a qualitatively similar way to water [e.g., Fig. 4(A)], and in this regard the lowest concentrations of Carbopol and the

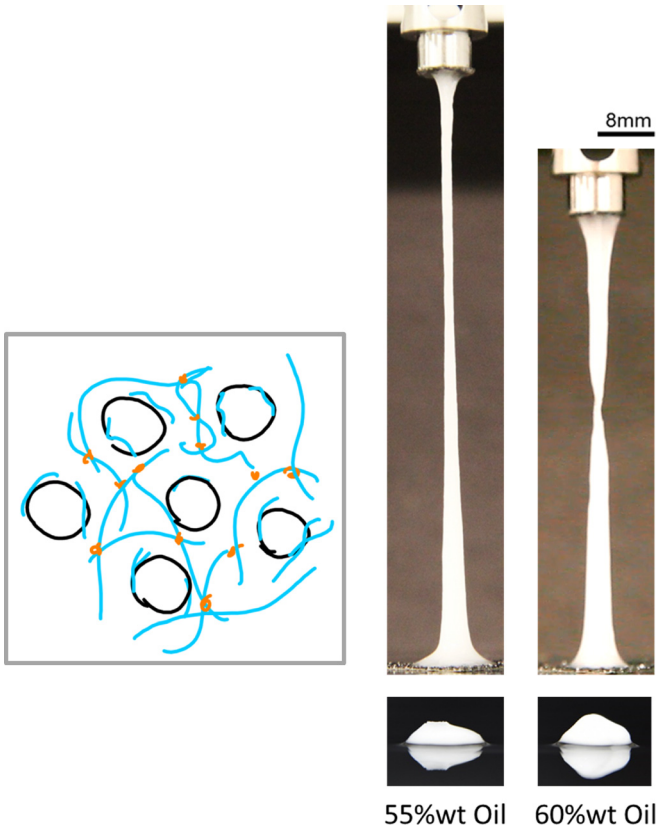

FIG. 9. Proposed highly extensible model yield-stress fluid, a silicone oil-in-water emulsion combined with a transiently crosslinked network of PVA (MW 85 000–124 000). Shown on the left is a sketch of the microstructural concept used to conceive of this material: The emulsified droplets (circles) provide the material with a structure with which to bear static loads (a yield stress), while the transiently crosslinked polymer network (lines with crosslinks at intersection points) prevents the droplets from coalescing and allows the structure to survive large extensional strains. Shown on the right are the two synthesized formulations which manifested the desired qualitative performance objectives. The 8 mm scale bar shown applies to all four images on the right.

silicone oil-in-water emulsion (repulsion-dominated systems) have strain-to-break values slightly below the indicated water break-up limit under zero gravity of 135% determined for our initial volume from Sanz and Martinez [50]. The surface tension of water was used to calculate the values taken from simulations for the 3D tensorial Herschel-Bulkley model [13], as all of our material systems have a continuous water-phase. For those simulations, an aspect ratio of $\Lambda_0 = 2$ was used and thus a smaller strain-to-break is expected. The simulations show nonmonotonic behavior of ε_{break} versus σ_Y , with ε_{break} varying by at most a factor of two for the shown range of yield stresses, similar to the variation in the archetypal materials. For these archetypal materials, we find that the least extensible materials belong to the repulsion-dominated category, while the highest extensibility is achieved by an attraction-dominated material composed of long-chain polymers.

As shown in Fig. 1, when considering application-relevant materials, the strain limit for the filament-stretching experimental method was reached for some materials and thus it was necessary to make use of the counter-rotating-drum experimental setup shown in Fig. 7. As pointed out in

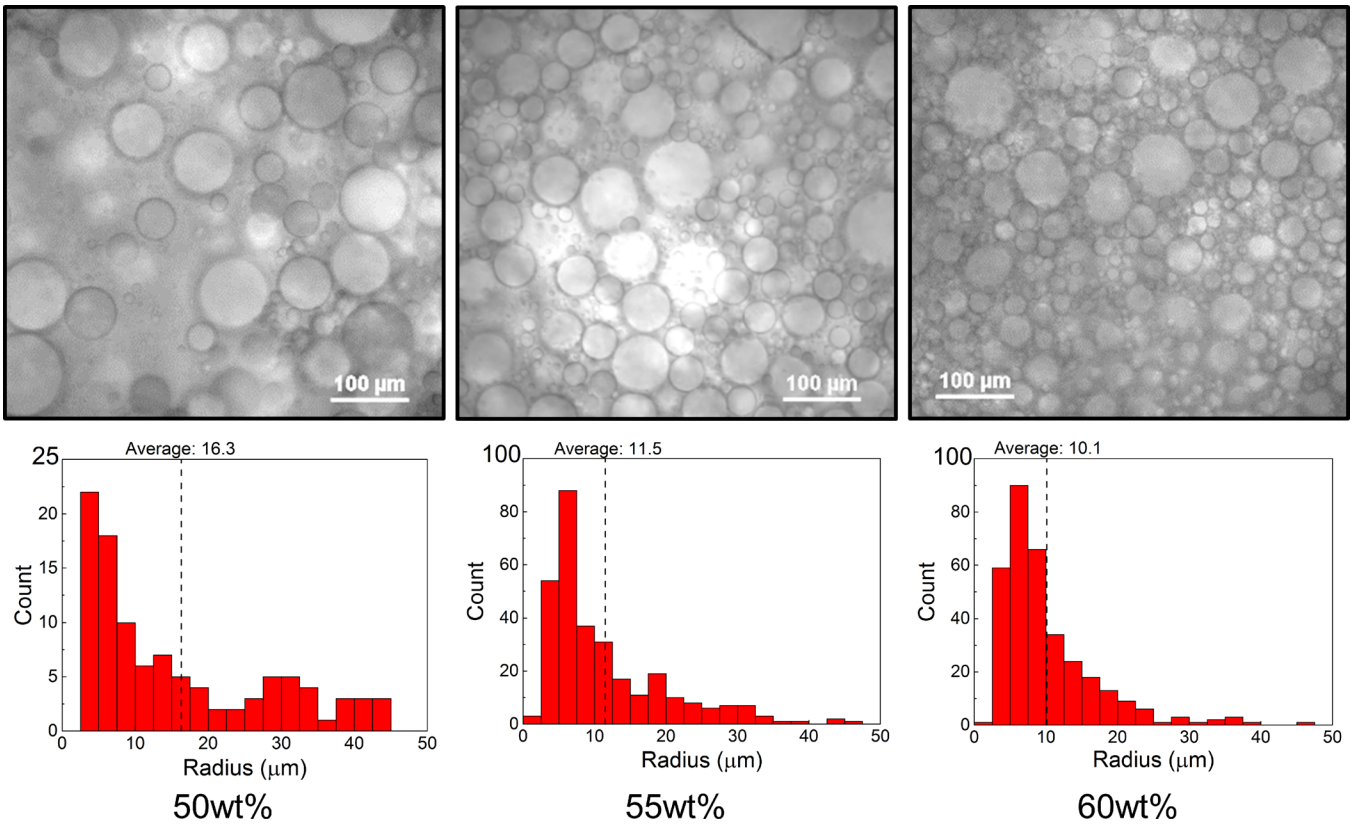

FIG. 10. Micrographs and droplet size distributions of the designed PVA-borax emulsion at different oil content formulations. The 50 wt. % formulation has areas of the microstructure with relatively loose packing of oil droplets, whereas the 55 wt. % and 60 wt. % formulations always have a high oil-droplet packing. The droplet size distributions were quantified using the resolvable droplets in the images shown.

Sec. II A, ε_{break} is an *extrinsic* material property that may depend on the initial geometry. Thus, one should not necessarily expect consistency when comparing between the filament-stretching and counter-rotating-drum setups. In the particular cases of the consumer products tested here (Laffy Taffy and Hubba Bubba Tape), there is some consistency in the fact that ε_{break} on the counter-rotating-drum setup is larger than the maximum strain of the filament stretching setup.

Comparing the consumer products to the archetypal fluids in Fig. 8, while the laboratory systems approach the behaviors of Nutella and whipped frosting, they come nowhere near the HexArmor resin, Mystic Smoke, or confectionary products. Thus, archetypal model materials and mathematical constitutive models may be irrelevant for understanding of some materials in applications in which physics associated with both yield stress and high extensibility is required.

B. Design and analysis of a model material

In attempting to match the performance of materials shown in Figs. 1(B) and 1(C) with that of a model material, we followed a methodology for the design of a yield-stress fluid described in [19]. The design methodology contrasts with analysis strategies in that it is built upon generic principles of inverse problem solving: The performance objective (material behavior) is specified in a chemistry- and structure-agnostic way, allowing for creative concept generation. Ideally, one would be able to select materials matching the necessary properties from a material database. However, since the paradigm of highly extensible yield-stress fluids is underdeveloped, we carried out the analysis/characterization (described in Sec. IV A) ourselves. Because as we have shown, none of the surveyed archetypal yield-stress fluids could achieve the properties or performance displayed by the application-relevant materials, our only choice was to formulate a new material. For this new material, we sought to make it a *model* highly extensible yield-stress fluid. We define a model material as (i) having a simple, controllable formulation; and (ii) having an interrogatable microstructure.

For this process, numerous microstructure concepts were envisioned using a technique of juxtaposing two different existing microstructures [19,51]. The material concept we chose to develop is shown in Fig. 9 and was conceived of as the combination of a yield-stress-providing microstructure (a packed emulsion) and an extensibility-providing microstructure (a transiently crosslinked network).

An emulsion was chosen as the yield-stress-providing microstructure since it conceptually allows for the compartmentalization of different additives into the water (continuous) and oil (dispersed) phases, thus allowing for more freedom when choosing the method of providing high extensibility. As stated, one of the preferred goals was for the model system to have a simple formulation. For this reason, poly(vinyl-alcohol) with a moderately high molecular weight was chosen to provide the extensibility since it has dual functionality as an emulsifier, removing the need for an

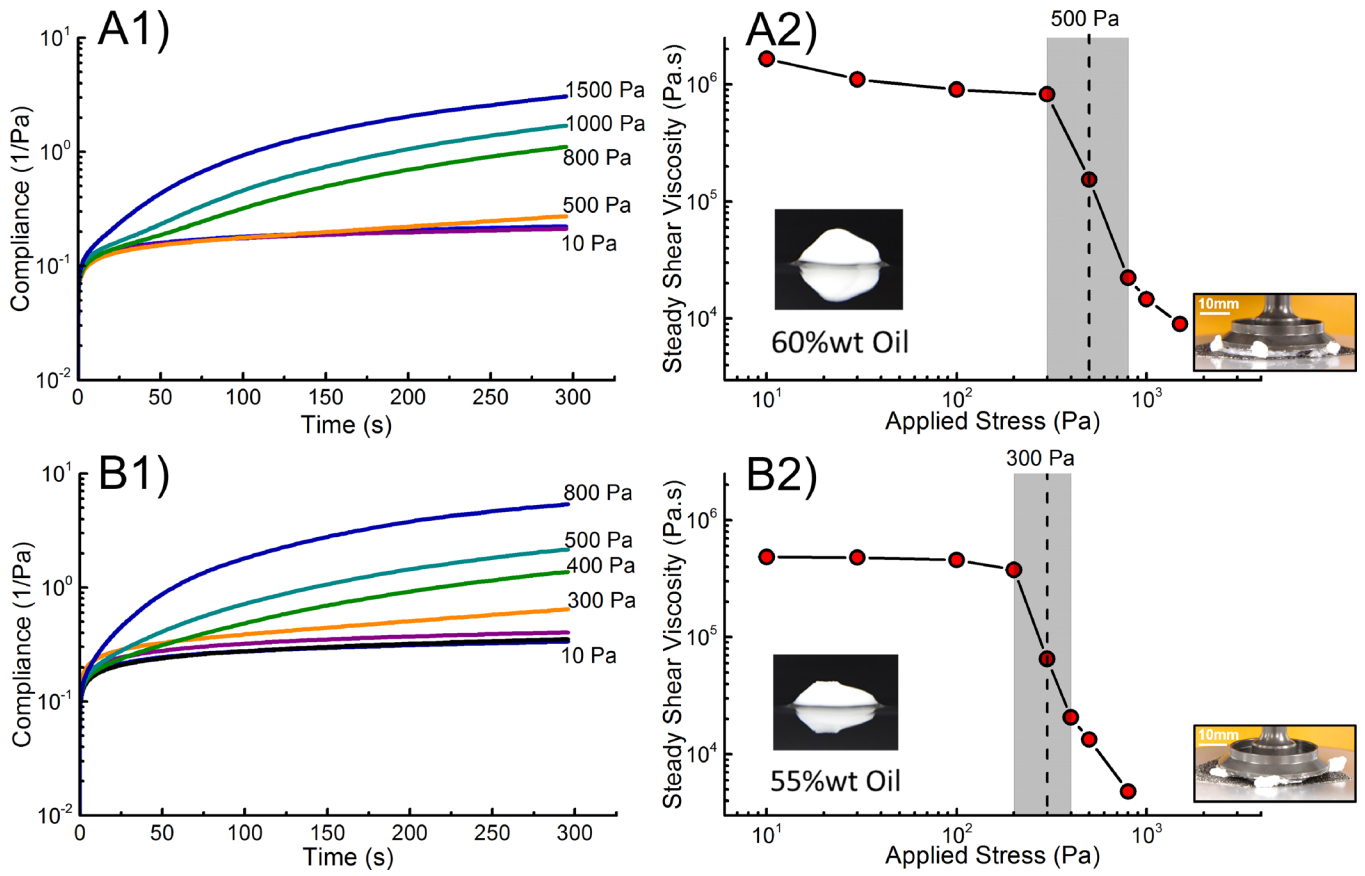

FIG. 11. Shear creep compliance curves for two formulations of the proposed model material with (A) 60 and (B) 55 wt. % silicone oil. Compliance over time at various levels of applied stress (A1) and (B1), resulted in steady shear viscosity curves (A2) and (B2) which show yielding. The gray shaded regions are bounded by the stresses over which viscosity decreases by over half an order of magnitude, the yield stress for each material is taken as the stress for the data point within the shaded regions. Inset images depict sample fracture which occurs at stresses higher than the reported data points.

additional emulsifying ingredient. To further increase the extensibility, we chose to add borax as a transient cross-linker; an alternative strategy for increasing extensibility might be to use a very high molecular weight poly(vinyl-alcohol), but in practice this made emulsification more difficult and this strategy was not pursued.

As desired of our model system, the microstructure is directly observable. Images of the microstructure obtained by microscopy and measurements of the radii of the resolvable droplets in the respective images are shown in Fig. 10 for a range of oil content. As envisioned, there exists a dispersed oil droplet microstructure which packs together, providing a mechanism for yield-stress behavior to occur. Figure 10 shows that some areas of the 50 wt. % formulation (which did not show yield-stress behavior, see Supplementary Material) are relatively open with few oil droplets. This is not the case for the 55 and 60 wt. % formulations which always have significant oil-droplet packing. From the measurements of droplet radii of the 50, 55, and 60 wt. % images, the mean droplet sizes were 16.3, 11.5, and 10.1 μm, respectively. For the same measurements fit to a lognormal distribution, the lognormal means were 2.5, 2.2, and 2.1 μm, respectively. For either distribution, the mean droplet radius does not decrease significantly with increasing oil content. Including droplets outside of the frame shown in Fig. 10 (see Supplementary Material), the maximum droplet radii with increasing oil content were 105, 64, and 75 μm, respectively, and again no clear trend is seen. The smallest measured droplet radius across all samples was 2.4 μm, but it is likely that smaller but unresolvable droplets exist within all samples.

With this microscopy technique, we are unable to view the structure of the PVA; however, PVA is known to move to the interface of oil and water [44]. Since we are unable to determine any microstructure composed of PVA and Borax, it is unknown how accurately our formulated material matches our synthesized design concept. However, based on this concept, we were able to achieve the performance shown in Fig. 9, which can match the extensibility of existing consumer products.

Figure 11 shows the shear creep compliance characterization for the PVA-borax emulsions with two different oil loadings. Above 50 wt. % oil (Supplementary Material Fig. S24), the material transitions from a shear-thinning material with no yield stress to a yield-stress fluid with yield stresses of 300 and 500 Pa for the 55 and 60 wt. % oil formulations, respectively.

Though these materials can achieve the yield stress performance objectives we sought, there are numerous experimental challenges with the system including edge fracture at high stresses or shear rates (Fig. 11 inset), and a propensity toward slip and confinement artifacts (see Supplementary Material for discussion).

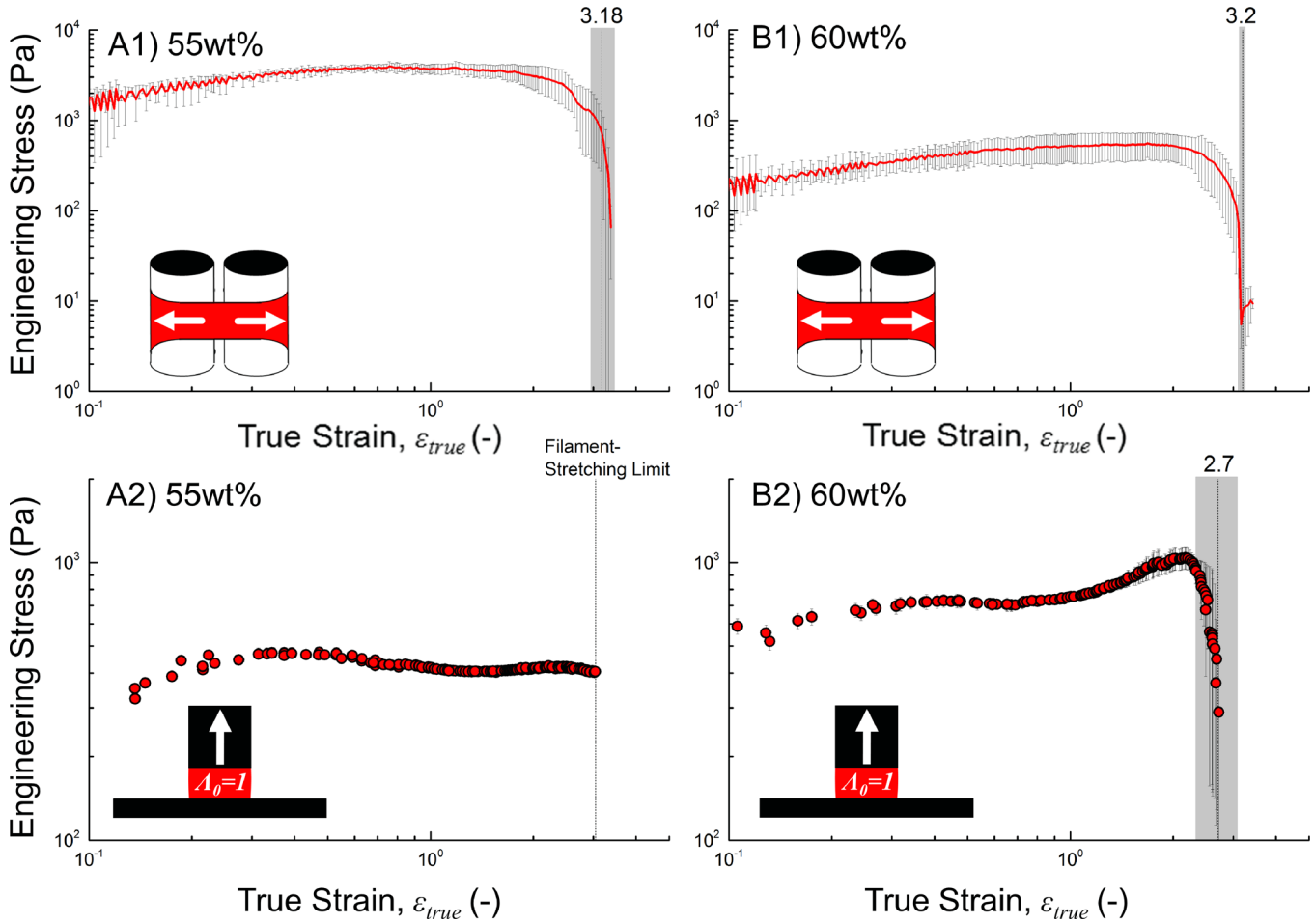

FIG. 12. Extensional engineering stress curves for the proposed model highly extensible yield-stress fluid. (A) 55 wt. % and (B) 60 wt. % formulation. (A1) and (B1) depict experiments performed using the SER3 experimental setup with the average of repeated experiments in red and error bars in gray. (A2) and (B2) depict experiments performed using the ARES-G2 experimental setup. Curves were correlated with video to determine the engineering strain-to-break. For subsequent figures, values of strain-to-break are taken from (A1) and (B1). Error bars shown are the standard deviation from repeated experiments.

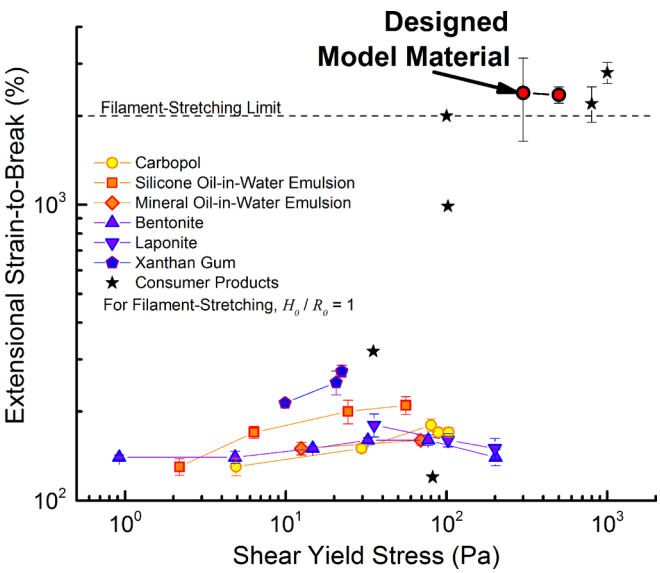

FIG. 13. Ashby-style co-plot of all materials studied here. For data points above the filament-stretching limit, values from the counter-rotating-drum setup were used. See Supplementary Material for the full steady shear flow and extensional engineering stress curves that these points represent. Error bars shown are the standard deviation from repeated experiments.

Figure 12 shows the characterization of the PVA-borax emulsions in extension in both the filament-stretching and counter-rotating-drum experimental setups. As was desired for matching the behavior of the application-relevant products, the 55 wt. % oil reached the strain-limit of the filament-stretching setup [Fig. 12(A2)], and thus necessitated testing on the counter-rotating-drums. Due to the softness of the material, reproducible loading for this setup was extremely challenging for both formulations, resulting in the standard deviation error bars shown. The 60 wt. % formulation was the only observed material that was capable of being tested on both experimental setups. For comparison between the two formulations, the strain-to-break values were both taken from the counter-rotating-drum setup (A1 and B1).

In Fig. 13, characterization results for the designed yield-stress fluid system are shown compared to archetypal and consumer/industrial yield-stress fluids. With our synthesized material, we are able to match the extensibility performance of the most extensible consumer products shown here.

V. CONCLUSIONS

Here, we have presented a new paradigm of yield-stress fluids as capable of being highly extensible materials. We

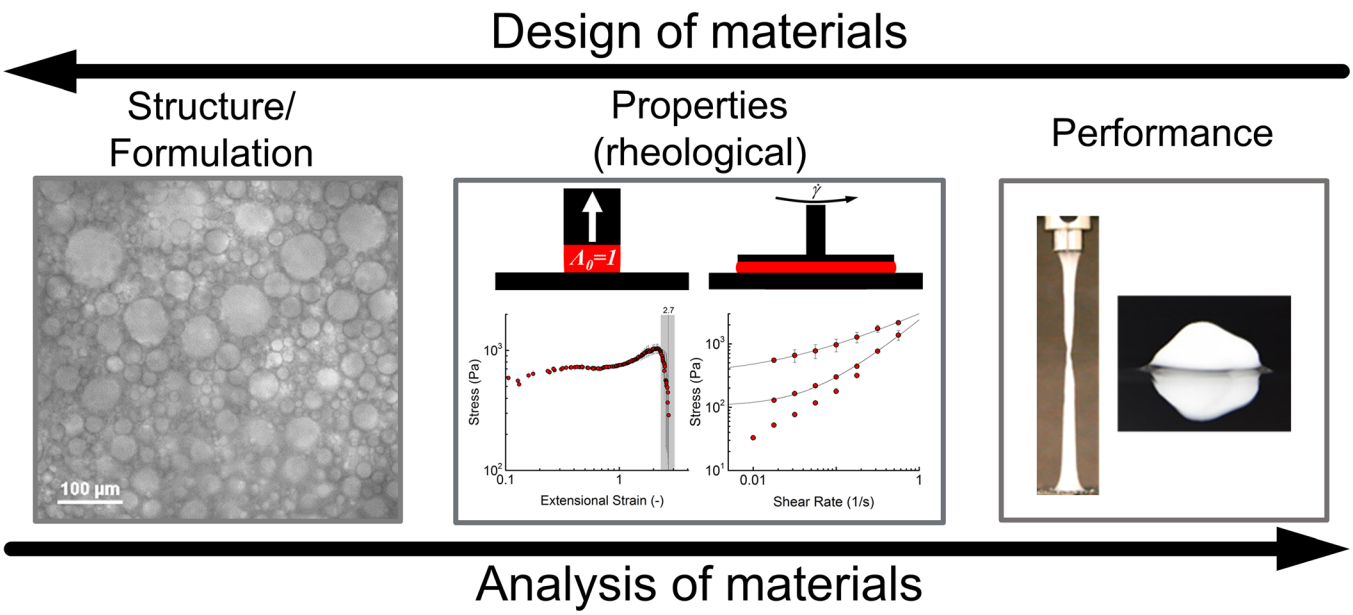

FIG. 14. Schematic relations of design and analysis of materials (adapted from [52] and applied to rheological properties). The process presented in this work demonstrates the complementary nature of analysis and design. Starting with the observable performance goal (on the right) of yield-stress fluids that are highly extensible [Figs. 1(B) and 1(C)], attempts were made to match this by analyzing and evaluating simple model systems (Fig. 2); when this failed a new microstructure concept was conceived and formulated (on left, also Fig. 9), and analyzed for validation that the performance goal had been met. Following these principles, we have demonstrated the design process of a new material that is built upon a strong foundation of analysis.

introduced a methodology for characterizing yield-stress fluids capable of capturing a wide range of yield stress and extensibility behavior. Lacking a suitable model highly extensible yield-stress fluid, we generated a concept for a new material based on a combination of microstructures, synthesized our candidate material, and then carried out rheological characterization. Though there are numerous experimental challenges associated with the newly synthesized material, we have shown that it is capable of quantitatively matching the behavior of highly extensible yield-stress fluid consumer products. Schematic relations of the design and analysis processes we carried out are shown in Fig. 14.

We have shown here that the archetypal yield-stress fluids are not acceptable models when studying materials where high extensibility is important, and we have provided a candidate model material for study. However, we have also shown that the inverse is true: When studying applications where a low extensibility is preferred or expected, one may choose from many well-characterized model materials and need not worry about the physics associated with high extensibility. For the high-extensibility materials, new constitutive models are required that capture the appropriate physics. In order to satisfy the Considère criterion, a candidate constitutive model would have to capture yield-stress fluid behavior as well as viscoelasticity and extension-rate dependence [53,54]. As stated when introducing our characterization method, the results are dependent on initial geometry and extension rate. Though our initial geometry was chosen to have a near-optimal initial aspect ratio, our choice of extension rate was somewhat arbitrary. It has yet to be investigated what effect extension rate would have on the materials tested here.

Shown here are only a few material formulations, and thus the full performance space available for our designed system is unknown and is certainly unoptimized—not to mention the plethora of unsynthesized or even unconsidered materials that may also match the target performance. Extremely high extensibility will also not be the intended target performance for different applications. For instance, the HexArmor resin [Fig. 1(B)] used in printing only reaches a moderate extensibility. We conjecture that the extensibility of this material contributes to a smoother extrusion or spraying process, but it is unknown where in the design space would be "ideal" for printing. Our characterization methodology provides a framework for determining areas of the design space that are consistent with ideal performance for applications where it is suspected that extensibility plays a role.

ACKNOWLEDGMENTS

This work was supported by the Wm. Wrigley Jr. Company and the National Science Foundation under Grant No. CMMI-1463203. The authors also thank Eric Klingenberg and Leslie Morgret for their support. A.Z.N. gratefully thanks J. Gerstmann, V. Caravella, A. Walker, R. Davis, D. Scanlon, A. Navarro, J. Oestreicher, B. Shoemaker, P. Klepek, J. Bakalar, A. Russell, B. Pack, and D. Ryckert for many thought-provoking conversations.

APPENDIX: CONSIDÈRE CRITERION WITH A GENERALIZED NEWTONIAN FLUID

This appendix provides a demonstration of the instability in extension of all Generalized Newtonian Fluid models (including Bingham and Herschel-Bulkley) according to the Considère criterion. This process has been used to predict the failure strain for constitutive equations that describe the

behavior of polymer melts [33]. The Considère criterion states that homogeneous uniaxial elongation occurs provided the strain is less than the strain at which the maximum of the force occurs. In other words, a material is stable in uniaxial extension in the Z-direction for

$$\frac{dF_z}{d\varepsilon} > 0, \tag{A1}$$

where F_z is the tensile force and ε is the applied true strain. For constant strain rate $\dot{\varepsilon}_0$,

$$\frac{dF_z}{d\varepsilon} = \frac{dF_z}{dt}\frac{1}{\dot{\varepsilon}_0} \tag{A2}$$

and for total stress tensor $\underline{\underline{\sigma}}(t)$, cross-sectional area $A(t)$, free surface in r-direction, and uniaxial extensional viscosity $\eta_u(t)$,

$$F_z(t) = [(\sigma_{zz}(t) - \sigma_{rr}(t)]A(t) = \dot{\varepsilon}_0\eta_u(t)A(t). \tag{A3}$$

Therefore,

$$\frac{dF_z}{d\varepsilon} = \eta_u(t)\frac{dA}{dt} + A(t)\frac{d\eta_u}{dt}. \tag{A4}$$

For an incompressible generalized Newtonian fluid model (i.e., $\underline{\underline{\sigma}} = \eta(\dot{\gamma})\underline{\underline{\dot{\gamma}}}$), where $\underline{\underline{\dot{\gamma}}} = \underline{\nabla v} + (\underline{\nabla v})^{\mathrm{T}}$, and $\dot{\gamma} = \sqrt{(1/2)\underline{\underline{\dot{\gamma}}} : \underline{\underline{\dot{\gamma}}}} = \sqrt{3}\dot{\varepsilon}_0 = \text{constant}$,

$$\frac{dA}{dt} < 0, \tag{A5}$$

$$\frac{d\eta_u}{dt} = 0. \tag{A6}$$

Therefore,

$$\frac{dF}{d\varepsilon} < 0 \tag{A7}$$

at all times. Therefore, for any assumed $\eta(\dot{\gamma})$, including the reformatted Herschel-Bulkley model where $\eta(\dot{\gamma}) = (\sigma_Y/\dot{\gamma}) + (\sigma_Y/\dot{\gamma}_{critical})\dot{\gamma}^{n-1}$, stable uniaxial elongation is never guaranteed.

References

[1] Bonn, D., M. M. Denn, L. Berthier, T. Divoux, and S. Manneville, "Yield stress materials in soft condensed matter," Rev. Mod. Phys. **89**, 035005 (2017).

[2] Barnes, H. A., "The yield stress—A review or 'panta rhei'—Everything flows?," J. Non-Newtonian Fluid Mech. **81**, 133–178 (1999).

[3] Sun, A., and S. Gunasekaran, "Yield stress in foods: Measurements and applications," Int. J. Food Prop. **12**, 70–101 (2009).

[4] Compton, B. G., and J. A. Lewis, "3D-printing of lightweight cellular composites," Adv. Mater. **26**, 5930–5935(2014).

[5] Ewoldt, R. H., C. Clasen, A. E. Hosoi, and G. H. McKinley, "Rheological fingerprinting of gastropod pedal mucus and synthetic complex fluids for biomimicking adhesive locomotion," Soft Matter **3**, 634–643 (2007).

[6] Balmforth, N. J., I. A. Frigaard, and G. Ovarlez, "Yielding to stress: Recent developments in viscoplastic fluid mechanics," Annu. Rev. Fluid Mech. **46**, 121–146 (2014).

[7] Coussot, P., "Yield stress fluid flows: A review of experimental data," J. Non-Newtonian Fluid Mech. **211**, 31–49 (2014).

[8] Møller, P., A. Fall, V. Chikkadi, D. Derks, and D. Bonn, "An attempt to categorize yield stress fluid behaviour," Philos. Trans. A. Math. Phys. Eng. Sci. **367**, 5139–5155 (2009).

[9] Martinetti, L., A. M. Mannion, W. E. Voje, R. Xie, R. H. Ewoldt, L. D. Morgret, F. S. Bates, and C. W. Macosko, "A critical gel fluid with high extensibility: The rheology of chewing gum," J. Rheol. (N. Y. N. Y). **58**, 821–838 (2014).

[10] Rutz, A. L., K. E. Hyland, A. E. Jakus, W. R. Burghardt, and R. N. Shah, "A multimaterial bioink method for 3D printing tunable, cell-compatible hydrogels," Adv. Mater. **27**, 1607–1614 (2015).

[11] Barral, Q., G. Ovarlez, X. Chateau, J. Boujlel, B. Rabideau, and P. Coussot, "Adhesion of yield stress fluids," Soft Matter **6**, 1343–1351 (2010).

[12] Coussot, P., and F. Gaulard, "Gravity flow instability of viscoplastic materials: The ketchup drip," Phys. Rev. E. **72**, 031409 (2005).

[13] Balmforth, N. J., N. Dubash, and A. C. Slim, "Extensional dynamics of viscoplastic filaments: II. Drips and bridges," J. Non-Newtonian Fluid Mech. **165**, 1147–1160 (2010).

[14] Boujlel, J., and P. Coussot, "Measuring the surface tension of yield stress fluids," Soft Matter **9**, 5898–5908 (2013).

[15] Aytouna, M., J. Paredes, N. Shahidzadeh-Bonn, S. Moulinet, C. Wagner, Y. Amarouchene, J. Eggers, and D. Bonn, "Drop formation in non-Newtonian fluids," Phys. Rev. Lett. **110**, 1–5 (2013).

[16] Niedzwiedz, K., H. Buggisch, and N. Willenbacher, "Extensional rheology of concentrated emulsions as probed by capillary breakup elongational rheometry (CaBER)," Rheol. Acta **49**, 1103–1116 (2010).

[17] German, G., and V. Bertola, "The free-fall of viscoplastic drops," J. Non-Newtonian Fluid Mech. **165**, 825–828 (2010).

[18] Martinie, L., H. Buggisch, and N. Willenbacher, "Apparent elongational yield stress of soft matter," J. Rheol. (N. Y. N. Y) **57**, 627–646 (2013).

[19] Nelson, A. Z., and R. H. Ewoldt, "Design of yield-stress fluids: a rheology-to-structure inverse problem," Soft Matter **13**, 7578–7594 (2017).

[20] McKinley, G. H., and T. Sridhar, "Filament-stretching rheometry of complex fluids," Annu. Rev. Fluid Mech. **34**, 375–415 (2002).

[21] Sentmanat, M. L., "Miniature universal testing platform: From extensional melt rheology to solid-state deformation behavior," Rheol. Acta **43**, 657–669 (2004).

[22] Hoyle, D. M., and S. M. Fielding, "Criteria for extensional necking instability in complex fluids and soft solids. Part II imposed tensile stress and force protocols,"J. Rheol. **60**, 1347–1375 (2016).

[23] Yao, M., and G. H. McKinley, "Numerical simulation of extensional deformations of viscoelastic liquid bridges in filament stretching devices," J. Non-Newtonian Fluid Mech. **74**, 47–88 (1998).

[24] Malkin, A. Y., and C. J. S. Petrie, "Some conditions for rupture of polymer liquids in extension," J. Rheol. (N. Y. N. Y) **41**, 1–25 (1997).

[25] Bhat, P. P., S. Appathurai, M. T. Harris, M. Pasquali, G. H. McKinley, and O. A. Basaran, "Formation of beads-on-a-string structures during break-up of viscoelastic filaments," Nat. Phys. **6**, 625–631 (2010).

[26] Galindo-Rosales, F. J., J. P. Segovia-Gutiérrez, F. T. Pinho, M. A. Alves, and J. de Vicente, "Extensional rheometry of magnetic dispersions," J. Rheol. (N. Y. N. Y) **59**, 193–209 (2015).

[27] Sentmanat, M., "High rate extensional flow behavior of confectionery products - objectifying 'mouthfeel'," in Soc. Rheol. Annu. Meet. (2007).
[28] McKinley, G. H., and A. Tripathi, "How to extract the Newtonian viscosity from capillary breakup measurements in a filament rheometer," J. Rheol. (N. Y. N. Y) **44**, 653–670 (2000).
[29] Rees, D., *Basic Engineering Plasticity: An Introducting With Engineering and Manufacturing Applications*, Boston, MA (Elsevier, 2006).
[30] Considère, M., "Memoire sur l'emploi du fer et de l'acier dans les constructions," Ann. Des Ponts Chausées **9**, 574–775 (1885).
[31] Vincent, P. I., "The necking and cold-drawing of rigid plastics," Polymer (Guildf) **1**, 7–19 (1960).
[32] Hutchinson, J. W., and H. Obrecht, "Tensile instabilities in strain-rate dependent materials," Fracture **1**, 101–116 (1977).
[33] McKinley, G. H., and O. Hassager, "The Considère condition and rapid stretching of linear and branched polymer melts," J. Rheol. (N. Y. N. Y) **43**, 1195–1212 (1999).
[34] Hibbeler, R. C., *Mechanics of Materials*, Boston, MA (Pearson Prentice Hall, 2014).
[35] Macosko, C. W., *Rheology Principles, Measurements, and Applications* (Wiley, New York, 1994).
[36] Nguyen, Q. D., and D. V. Boger, "Measuring the flow properties of yield stress fluids," Annu. Rev. Fluid Mech. **24**, 47–88 (1992).
[37] Møller, P. C. F., J. Mewis, and D. Bonn, "Yield stress and thixotropy: on the difficulty of measuring yield stresses in practice," Soft Matter **2**, 274–283 (2006).
[38] Burmistrova, A., and R. von Klitzing, "Control of number density and swelling/shrinking behavior of P(NIPAM–AAc) particles at solid surfaces," J. Mater. Chem. **20**, 3502–3507 (2010).
[39] Clasen, C., B. P. Gearing, and G. H. McKinley, "The flexure-based microgap rheometer (FMR)," J. Rheol. (N. Y. N. Y) **50**, 883–905 (2006).
[40] Le Merrer, M., R. Lespiat, R. Höhler, and S. Cohen-Addad, "Linear and non-linear wall friction of wet foams," Soft Matter **11**, 368–381 (2015).
[41] Weitz, D. A., and J. S. Huang, "Self–similar structures and the kinetics of aggregation of gold colloids," in *Kinet. Aggreg. Gelation*, New York (Elsevier, 1984), pp. 19–28.
[42] Liu, Y. D., and H. J. Choi, "Electrorheological fluids: Smart soft matter and characteristics," Soft Matter **8**, 11961–11978 (2012).
[43] Mickel, W., S. Münster, L. M. Jawerth, D. A. Vader, D. A. Weitz, A. P. Sheppard, K. Mecke, B. Fabry, and G. E. Schröder-Turk, "Robust pore size analysis of filamentous networks from three-dimensional confocal microscopy," Biophys. J. **95**, 6072–6080 (2008).
[44] Biehn, G. F., and M. L. Ernsberger, "Polyvinyl alcohol as an emulsifying agent," Ind. Eng. Chem. **40**, 1449–1453 (1948).
[45] Joshi, Y. M., "Model for cage formation in colloidal suspension of laponite," J. Chem. Phys. **127**, 081102 (2007).
[46] Ewoldt, R. H., M. T. Johnston, and L. M. Caretta, "Experimental challenges of shear rheology with case studies in biological complex fluids," in *Complex Fluids Biol. Syst.*, New York, edited by S. E. Spagnolie (Springer, 2015), pp. 207–241.
[47] Meeker, S. P., R. T. Bonnecaze, and M. Cloitre, "Slip and flow in pastes of soft particles: Direct observation and rheology," J. Rheol. (N. Y. N. Y) **48**, 1295–1320 (2004).
[48] Coussot, P., Q. D. Nguyen, H. T. Huynh, and D. Bonn, "Viscosity bifurcation in thixotropic, yielding fluids," J. Rheol. (N. Y. N. Y) **46**, 573–589 (2002).
[49] See Supplementary Material at https://doi.org/10.1122/1.5003841 for full shear and extensional data, additional discussion of experimental artifacts observed with the proposed model material, as well as videos of materials in extension.
[50] Sanz, A., and I. Martinez, "Minimum volume for a liquid bridge between equal disks," J. Colloid Interface Sci. **93**, 235–240 (1983).
[51] de Bono, E., *Lateral Thinking* (Penguin Books, New York, NY, 1977).
[52] Olson, G. B., "Designing a new material world," Science **288**, 993–998 (2000).
[53] Maki, K. L., and Y. Renardy, "The dynamics of a viscoelastic fluid which displays thixotropic yield stress behavior," J. Non-Newtonian Fluid Mech. **181–182**, 30–50 (2012).
[54] Renardy, Y., and H. V. Grant, "Stretch and hold: The dynamics of a filament governed by a viscoelastic constitutive model with thixotropic yield stress behavior," Phys. Fluids **28**, 053104 (2016).